Chemical Engineering Science 138 (2015) 616–621

Contents lists available at ScienceDirect

Chemical Engineering Science

journal homepage: www.elsevier.com/locate/ces

Short Communication

Application of nanoporous graphene membranes in natural gas processing: Molecular simulations of CH_4/CO_2, CH_4/H_2S and CH_4/N_2 separation

Chengzhen Sun, Boyao Wen, Bofeng Bai *

State Key Laboratory of Multiphase Flow in Power Engineering, Xi'an Jiaotong University, Xi'an, Shaanxi 710049, China

HIGHLIGHTS

- Nanoporous graphene is a very promising gas separation membrane.
- Separation of CH_4/CO_2, CH_4/H_2S and CH_4/N_2 gas mixtures is very efficient.
- Appropriate pore size and geometry can achieve high permeability and selectivity.
- Performance of NPG membranes far surpasses the conventional polymer membranes.

GRAPHICAL ABSTRACT

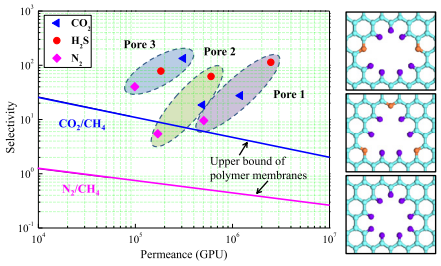

ARTICLE INFO

Article history:
Received 13 May 2015
Received in revised form
25 August 2015
Accepted 26 August 2015
Available online 12 September 2015

Keywords:
Nanoporous graphene
Membrane separation
Natural gas processing
Molecular dynamics
Permeability

ABSTRACT

Nanoporous graphene is a very promising gas separation membrane with ultrahigh permeability and selectivity. We demonstrate from molecular dynamics insights that the nanoporous graphene membranes with appropriate pore size and geometry can achieve high permeability and selectivity for separating CH_4/CO_2, CH_4/H_2S and CH_4/N_2 mixtures. For the 12-graphene-ring-units nanopores functionalized by N and H atoms, the permeance of CO_2, H_2S and N_2 are on the order of 10^5–10^6 GPU (gas permeation unit); the selectivity of permeating gases (*i.e.* CO_2, H_2S and N_2) over the non-permeating gases (*i.e.* CH_4) is as high as 10^2. The separation performance of the nanoporous graphene membranes for the three gas mixtures far surpasses the upper bond of the conventional polymer membranes. We anticipate that the development of nanoporous graphene membranes will provide a novel and high efficiency membrane separation technology for the natural gas processing and other gas separation processes in the industries.

1. Introduction

Natural gas is one of the most important energy sources, featuring high calorific value, high efficiency and low pollution. Raw natural gas contains many different components and varies distinctly in composition from source to source. Natural gas contains methane (typically 75–90% of the total) and other hydrocarbons, *e.g.* ethane, propane and butane. In addition, the gas contains some undesirable impurities, *e.g.* water, nitrogen, carbon dioxide, and hydrogen sulfide. For the transportation safety, the composition of natural gas delivered to the commercial pipeline grids is tightly controlled. Thus, a natural gas processing must be conducted before it enters the pipelines, which mainly involves the gas separation processes. There are many technologies to perform the gas separation process, including cryogenic separation, absorption/adsorption separation, supersonic separation and membrane separation, *etc.* In natural gas processing, membrane separation technology is widely used owing to its low energy cost, high

* Corresponding author.
E-mail address: bfbai@mail.xjtu.edu.cn (B. Bai).

http://dx.doi.org/10.1016/j.ces.2015.08.049
0009-2509/

efficiency and low pollution. It is usually employed to separate carbon dioxide, nitrogen, hydrogen sulfide and others from natural gas.

For the separation membranes, it was shown that the nanostructured materials exhibited better performance than the conventional polymer materials (Celebi et al., 2014; Dasgupta et al., 2015; Kim et al., 2013; Kwon and Jeong, 2015; Lee and Aluru, 2010; Li et al., 2013; Walker et al., 2015; Wang and Karnik, 2012; Xu et al., 2015; Zhao et al., 2014). Among them, nanoporous graphene (NPG) (Azamat et al., 2015; Bieri et al., 2009; Jiang et al., 2009; Jiao et al., 2013; Nieszporek and Drach, 2015; Schrier, 2010; Sun et al., 2015), a graphene sheet containing pores of size sub-nanometers, has been demonstrated as a very promising gas separation membrane, particularly due to its one-atomic thickness. At first, it was suggested theoretically that the NPG membranes exhibited ultrahigh permeability and selectivity far exceeding the existing state-of-the-art membranes by orders of magnitude. Schrier (Schrier, 2012) reported a CO_2 permeance of 4×10^5 GPU (gas permeation unit, 1 GPU$=3.35\times10^{-10}$ mol/s m^2 Pa) through a special porous graphene extended in one direction by an E-stilbene-like unit. Tao et al. (Tao et al., 2014) also found a high permeance of H_2, CO, N_2 and CH_4 for this special NPG membrane. Liu et al. (Liu et al., 2013a, 2013b) reported a permeance of H_2 in the range of 1×10^5–4×10^5 GPU and a permeance of CO_2 on the order of 10^5 GPU using molecular dynamics (MD) simulations. Lu et al. (2012) found a high selectivity for H_2 relative to CO, CH_4 and CO_2 through the graphene nanopores doped by B and N atoms. The permeation of gas molecules are affected by many factors, including the adsorption of molecules on graphene surface (Dai et al., 2009; Drahushuk and Strano, 2012; Du et al., 2011), the functionalization of pore rim and surface (Shan et al., 2012; Wu et al., 2014), the geometry distortion (Hauser and Schwerdtfeger, 2012) and the pore charge (Lei et al., 2014), *etc.* Huang et al. (2014) demonstrated that the permeance of H_2 (2.4×10^5 GPU) and selectivity ($\approx10^{24}$) were significantly improved for the separation of H_2/CH_4 with the development of an inter-layer-connected porous graphene bilayer. Wen et al. (2015) found that the gas permeability of NPG membranes could be inhibited by the non-permeating components of the gas mixtures. The gas molecular permeation mechanisms through the NPG membranes were revealed in our early work (Sun et al., 2014). We proposed that the total permeation flux is consisted of direct flux and surface flux.

Recently, some experimental studies were conducted to promote the realization of the conceptual NPG-based membranes. Koenig et al. (2012) measured the transport rates of a variety of gases, *i.e.* H_2, CO_2, Ar, N_2, CH_4 and SF_6, through a micrometer-sized NPG membrane and showed that the measured data was consistent with the theoretical models based on effusion through angstrom-sized pores. Celebi et al. (2014) reported a high transport rate for numerous gases across the physically perforated double-layer graphene featuring pores with narrowly distributed diameters. Boutilier et al. (2014) reported a systematic experimental and theoretical investigation on the gas transport through single- and multi-layer graphene membranes with intrinsic defects and revealed that a selective transport could be achieved in the presence of non-selective defects. This study further promoted the realization of practical and high-quality NPG-based gas separation membranes. All above researches have demonstrated that the NPG membrane is becoming a reality.

The studies on the application of NPG membranes in a practical gas separation process in the industries were very limited. Here, we discuss the potential application of NPG membranes in the separation of natural gas mixtures. We anticipate that the present work will give an opportunity to enable the NPG membranes to be applied in natural gas processing and others. Toward this end, we conduct a systematic and comprehensive theoretical study on the separation capability of NPG membranes for natural gas mixtures, including CH_4/CO_2, CH_4/H_2S and CH_4/N_2 mixtures. The MD simulation method is adopted, because it can accurately predict the atomic level transport phenomenon based on the movement of atoms/molecules. We employ three different nanopores functionalized by N and H atoms for each gas mixture. It is demonstrated that the NPG membranes with appropriate pore size and geometry can separate the gas mixtures with high permeability and selectivity. Although this work is conducted from the theoretical points of view and many challenges are faced currently for the application of NPG membranes in the industries, this work is valuable for showing the promise of NPG membranes in natural gas processing.

2. Simulation model

We performed the MD simulations in an equilibrium system, in which the graphene membrane of area 4×4 nm^2 divided the simulation box into two chambers with equal volume. The simulation box of height 30 nm contained 400 molecules for the gas mixtures, *i.e.* 200 for one component and 200 for the other component. Initially, there were 200 molecules arranged uniformly and alternately in each side to ensure an equal pressure. The simulations were performed using LAMMPS (Large-scale Atomic/Molecular Massively Parallel Simulator). Periodic boundary conditions were applied in the directions parallel to the graphene membrane, while reflective wall boundary conditions were applied in the direction perpendicular to the graphene membrane. In order to be more close to the real situation in the applications, the graphene sheet was not fixed, but vibrated during the simulation caused by the interactions with the gas molecules. For more details of the simulation system, one can refer to the Section 1 of Supplementary information. The simulations were run for 1.5×10^8 timesteps with a time step of 0.3 fs, involving a NVT ensemble at 300 K using a Nosé-Hoover thermostat. In the calculation, the electrostatic interactions among gas molecules and graphene membranes were specially considered due to the presence of polar molecules (*e.g.,* CO_2 and H_2S). The pair interactions among carbon and hydrogen atoms in the graphene were modeled by the AIREBO potential (the parameters were specified within the LAMMPS package). For carbon and hydrogen atoms, this potential model is more accurate than a simple Lennard-Jones potential. For the gas molecules, the atomic models were adopted. Apart from the AIREBO potential for CH_4, the preferable three-site model (Harris and Yung, 1995) with three partial charges was adopted for the polar CO_2 and H_2S (Lei et al., 2014; Liu et al., 2013a; Schrier, 2012), while the well-known Lennard-Jones potential was adopted to model the neutral N_2 (Du et al., 2011; Sun et al., 2014). The parameters for cross terms were evaluated by the Lorentz–Berthelot mixing rule. The bond stretch and bond angle deformation information of CH_4 was included in the AIREBO potential, while those of other gas molecules (*i.e.* N_2, CO_2 and H_2S) were all modeled by the harmonic type potential. The form and parameters of these potential models can be found in the Section 2 of Supplementary information. The cutoff distance for Lennard-Jones and Coulombic interactions was 10 Å.

We employed 3 functionalized nanopores (denoted as Pore 1, Pore 2 and Pore 3) to perform the separation process, as shown in Fig. 1. The three nanopores were created based on the 12-units pore, which contained 12 graphene ring units removed or partially opened. Pore 1 corresponds to two carbon atoms replaced with nitrogen atoms on the pore rim and single hydrogen atoms added to the other pore-rim carbon atoms; Pore 2 corresponds to three triangular distributed carbon atoms replaced with nitrogen atoms on the pore rim and single hydrogen atoms added to the other

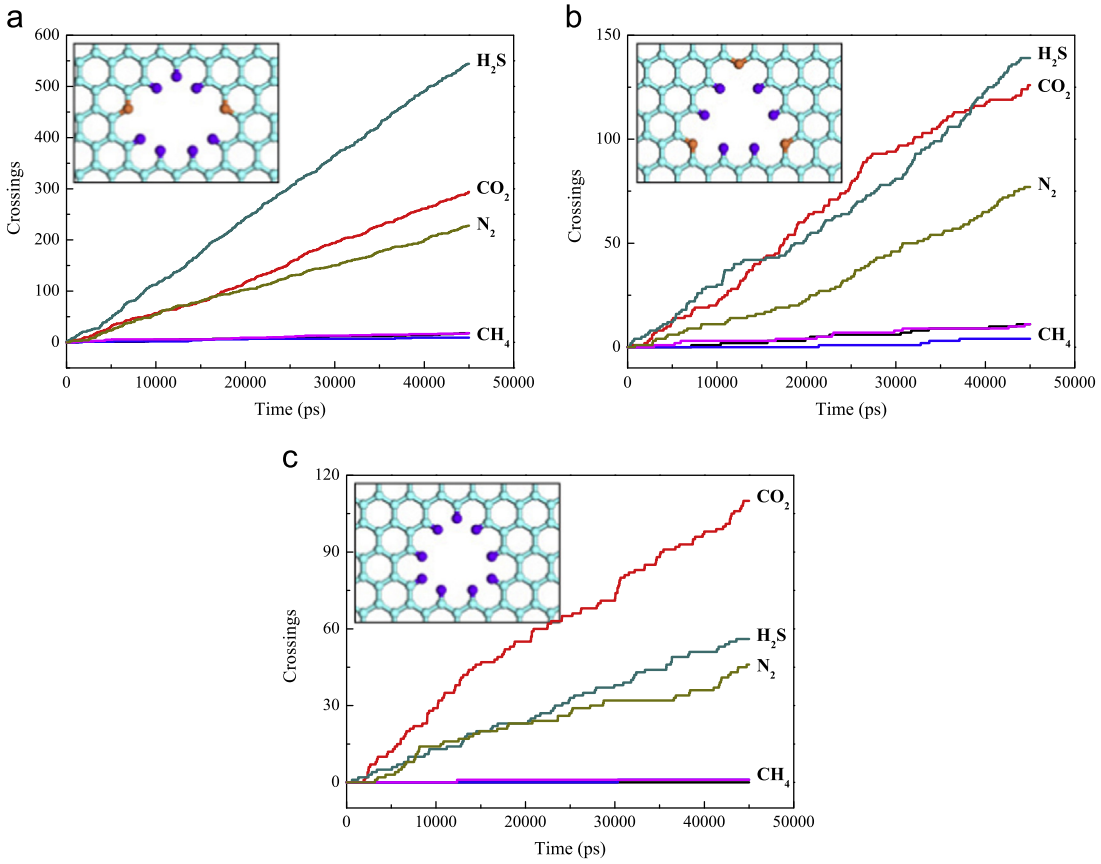

Fig. 1. Total bidirectional crossings *versus* time through the NPG membranes with different nanopores. (a) Pore 1; (b) Pore 2; (c) Pore 3. Light blue spheres denote C atoms in graphene, orange spheres denote the doped N atoms, and purple spheres denote the passivated H atoms. (For interpretation of the references to color in this figure legend, the reader is referred to the web version of this article.)

pore-rim carbon atoms; Pore 3 corresponds to single hydrogen atom added to each carbon atom on the pore rim. The values of the charges on the graphene membrane were obtained through a density functional theory calculation using the DMol^3 module in the Material Studio software. To save the computation cost, only the charges near the pores were considered, as shown in Fig. S2.

3. Results and discussion

3.1. Molecular crossing

During the simulation, the molecules can migrate from one side of the graphene to the other side by permeating through the nanopores (see Section 5 of Supplementary information). A molecule is considered to have crossed the graphene membrane if it moves from the bulk zone on one side to the bulk zone on the other side of the membrane, as illustrated in our previous work (Sun et al., 2014). In this study, an equilibrium system was employed and thus the molecular crossings in either direction (denoted as bidirectional crossings) during the entire simulation period were counted. It is noted that the permeate flux measured via bidirectional crossings in an equilibrium dilute system equals twice the flux in a non-equilibrium dilute system. We analyzed the molecular coordinates every 15,000 timesteps (4.5 ps), *i.e.* 10000 data points were collected to observe every possible crossing. The number of crossings increases linearly with time during the simulation (see Fig. 1), of which the slope can be adopted to obtain the permeation flux (in units of mol/m^{2}s based on the area of the graphene membrane). For the nanopores employed in this study, few crossings are observed for CH_4 because of its bigger size (especially for Pore 3, CH_4 has zero crossing), as shown in Fig. 1.

The observed crossings are different for the permeating gases (CO_2, H_2S and N_2) due to the distinct kinetic parameters of molecules, *i.e.* kinetic diameter and molecular mass, and the distinct adsorption abilities on the graphene surface. For Pore 1 and Pore 2, the number of crossings is in the order of $H_2S > CO_2 > N_2$; for Pore 3, CO_2 has a maximum crossing number while N_2 has a minimum crossing number. Although the kinetic diameters (H_2S: 0.360 nm and N_2: 0.364 nm) and the relative molecular masses (H_2S: 34 and N_2: 28) of H_2S and N_2 are comparable, H_2S has a bigger crossing number due to its stronger adsorption ability on the graphene surface (see below). For CO_2, the kinetic diameter (0.330 nm) is smallest while the relative molecular mass (44) is largest, resulting in a moderate permeation ability. Therefore, for the permeable pores, *i.e.* Pore 1 and Pore 2, the order of crossing number is $H_2S > CO_2 > N_2$. For the weakly permeable Pore 3, the permeation ability totally depends on the molecular diameter. Thus, the crossing number of CO_2 is the maximum while that of N_2 is the minimum. Meanwhile, we find that Pore 1 is the most permeable while Pore 3 is the worst, because the permeable area is different for the distinct chemical functionalizations by the N and H atoms. Pore 3 is the least permeable due to the blocking of the nine passivated H atoms, while Pore 1 is the most permeable because two longitudinal symmetrical passivated H atoms are replaced with doped N atoms, resulting in an elliptic permeable area.

3.2. Molecular adsorption

The gas molecules can strongly adsorb onto the graphene surface (the graphene membrane is located at $z=0$), which has a great impact on the molecular permeation, as illustrated in our early work (Sun et al., 2014). As shown in Fig. 2(a), the molecules have a high probability density in the regions $0.17\ \text{nm} < |z| < 0.6\ \text{nm}$ (denoted as adsorption layer). As $|z| > 0.6$ nm (bulk zone), the molecules have a uniform distribution along the z-direction. In the graphene zone ($|z| < 0.17$ nm), few molecules are confined in the nanopores, because only the molecules permeating through the nanopores appear in this zone. The molecular adsorption on the graphene surface is caused by the strong interactions between the graphene atoms and the gas molecules near the graphene surface. The adsorption intensity of different gases is different for the distinct interactions between the gas molecules and the graphene atoms. For example, owing to the stronger atomic interactions with the graphene, CO_2 molecules feature a higher density in the adsorption layer comparing with CH_4 molecules (see Fig. 2(a)). Fig. 2(b) displays the molecular number in the adsorption layers for various gases. As seen from the figure, H_2S possesses the densest adsorption layer, CO_2 takes second place, and the adsorption layer of N_2 is the sparsest. We note that the adsorbed molecular number of CH_4 in the CH_4/N_2 group is higher than those in the CH_4/CO_2 and CH_4/H_2S groups. This phenomenon is related to the weakly adsorbed N_2 molecules, more surface places are available for the CH_4 molecules to be adsorbed in the CH_4/N_2 group resulted by the competitive adsorption mechanisms. Meanwhile, the number of adsorbed molecules on the NPGs with Pore 3 is smaller than those on the NPGs with Pore 1 and Pore 2. This result can be attributed to the stronger interactions between the gas molecules and the doped N atoms in Pore 1 and Pore 2. In the adsorption layer, the molecules have a non-uniform distribution on the graphene surface due to the molecular permeation through the nanopores. As shown in Fig. 2(c), the CO_2 molecules have a low distribution in the regions near the pore, because the molecules near the pore migrate to the other side of the graphene and accordingly the density is lower than those in the zones far away from the pore. It is noted that in the center of the pore the molecules are concentrated because they are in line waiting to permeate through.

The molecular adsorption is beneficial for the molecular permeation. For the molecules with high adsorption intensity, apart from the molecular crossings directly from the bulk zone, plenty of molecules can cross the nanopores after being adsorbed on the graphene surface, as illustrated in our early work (Sun et al., 2014). Namely, these molecules firstly enter the adsorption layer and then migrate to the pore regions before they cross the membranes. This surface mechanism would have a great contribution on the total permeation flux of the strongly adsorbed gas molecules. As a molecule moving from one bulk zone to the other bulk zone, the probability distribution of the experience time during crossing, *i.e.* the time spends in the two adjacent adsorption layers and the graphene zone, are different for different molecules, as shown in Fig. 3. There are a few molecules in the adsorption layer for N_2, hence the molecules can easily migrate to the pore regions accompanied by few collisions with other molecules when they try to cross the nanopores from the adsorption layer. For CO_2 and H_2S, plenty of molecules appear in the adsorption layer; during the

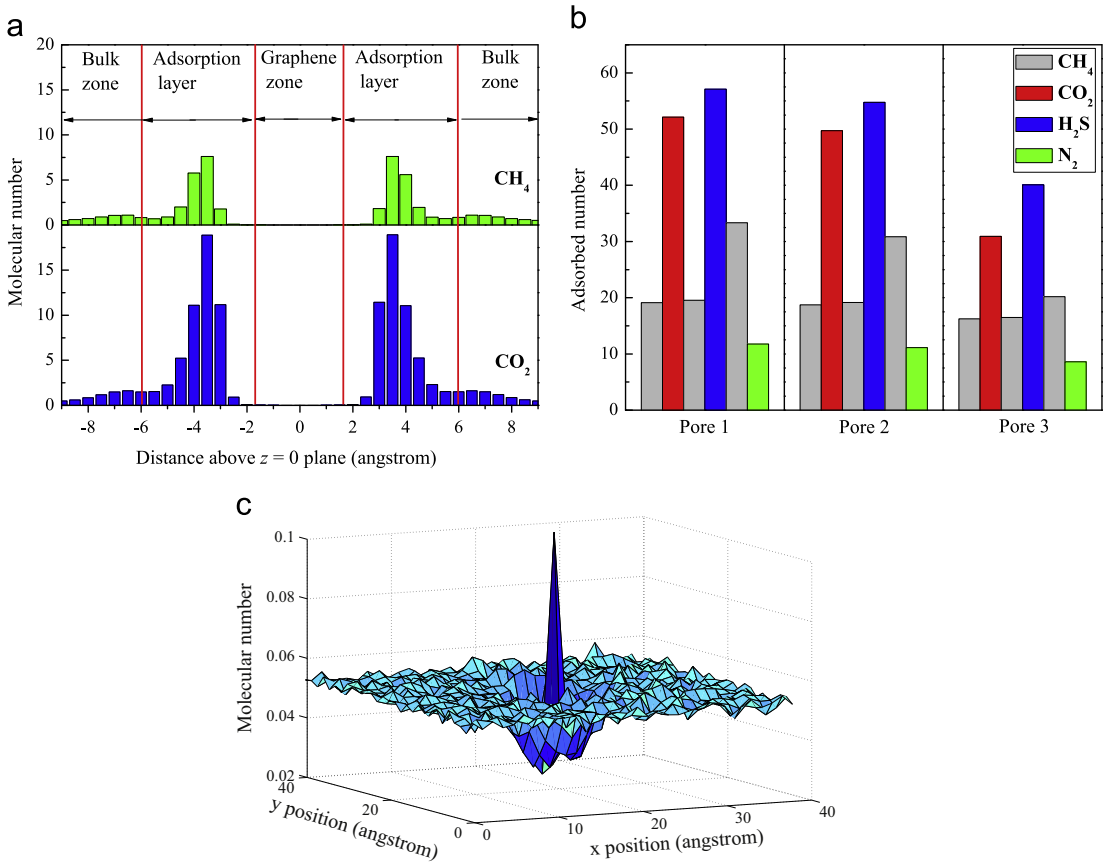

Fig. 2. Adsorption of molecules on the graphene surface. (a) Probability density of CH_4 and CO_2 molecules along the z-direction for the NPG with Pore 1; (b) the molecular number in the adsorption layer for different molecules at various graphene surfaces; (c) the surface density distribution of CO_2 molecules in the adsorption layer on the NPG with Pore 1. The coordinate value in this figure denotes the molecular number on the unit surface with an area of 1.74 Å^2.

molecular crossing from the adsorption layer, the molecules only can migrate to the pore regions after massive collisions with other molecules. Therefore, most of the crossings experience a long time period for CO_2 and H_2S; while the crossing can be happened in a short time period for N_2.

3.3. Permeance and selectivity

Although the experience time during crossing for N_2 is shortest, the permeation flux is not highest, because the total number of molecules waiting to permeate through the nanopore is different. The permeation flux across the membrane is calculated by averaging the bidirectional molecular crossings during the simulation period (see Fig. 1) and dividing by a factor of 2, as mentioned above. The permeance is obtained from the permeation flux normalized by the pressure of the gas phase. Due to the adsorption of gas molecules on the graphene surface, the gas phase pressure is calculated by considering only the molecules in the bulk zone ($|z| > 0.6$ nm) and the volume available to them. The pressures for the various gases are listed in Table S4; for the molecules with strong adsorption abilities, the gas phase pressures are much smaller than the initial nominal pressure (17.07 bar) of the system at the beginning of the simulation. In the calculations of permeance, the error bar is estimated based on a 95% confidence level using Poisson statistics (see the Section 4 of Supplementary information).

As shown in Fig. 4(a), the permeance of CO_2 and H_2S are higher than that of N_2 for all the pores in this study. For Pore 1 and Pore 2, the flux of H_2S is higher than that of CO_2; while for Pore 3 the flux of CO_2 is higher. We note that the fluxes of permeating gases (*i.e.* CO_2, H_2S and N_2) are on the order of 10^5–10^6 GPU and 1–2 orders of magnitude higher than those of non-permeating gases (*i.e.* CH_4). Thus, the selectivity of the permeating gases over the non-permeating gases is very high for the NPG membranes involved in this study, as shown in Fig. 4(b). Typically, the selectivity of N_2 over CH_4 is lower than those for the CO_2/CH_4 and H_2S/CH_4 groups. Meanwhile, we compare our results with the Robeson upper bound of polymer separation membranes (Robeson, 2008) and find that the data for NPG membranes far exceeds the upper bound of polymer membranes. It means that the NPG membranes can achieve a higher selectivity at higher permeance of permeating gases comparing to the conventional polymer membranes.

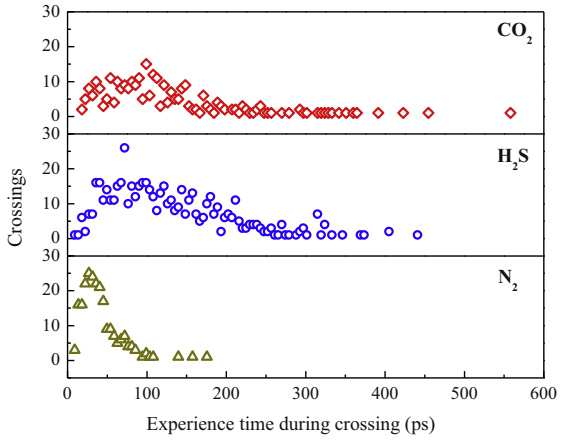

Fig. 3. Probability distribution of the experience time during the crossing for CO_2, H_2S and N_2 permeating through the NPG with Pore 1.

4. Conclusion

We have demonstrated from molecular dynamics insights that the NPG membranes with appropriate pore size and geometry can achieve high permeability and selectivity for separating the CH_4/CO_2, CH_4/H_2S and CH_4/N_2 mixtures. The permeance of CO_2, H_2S and N_2 are on the order of 10^5–10^6 GPU; the selectivity of permeating gases over non-permeating gases is as high as 10^2. The permeation ability of gas molecules has a great dependence with the molecular kinetic parameters and the adsorption on the graphene surface. A competitive adsorption mechanism on the graphene surface exists between the two components of the binary mixtures. In the adsorption layer, the molecules distribute non-uniformly due to the molecular permeation through the nanopores. For the molecules with different adsorption abilities, the probability distribution of the experience time during crossing is different. The separation performance of NPG membranes is far better than the conventional polymer membranes. We must note that this study was just conducted from theoretical points of view, the experimental works are urgently needed to facilitate the application of NPG membranes in the practical gas separation processes, such as natural gas processing.

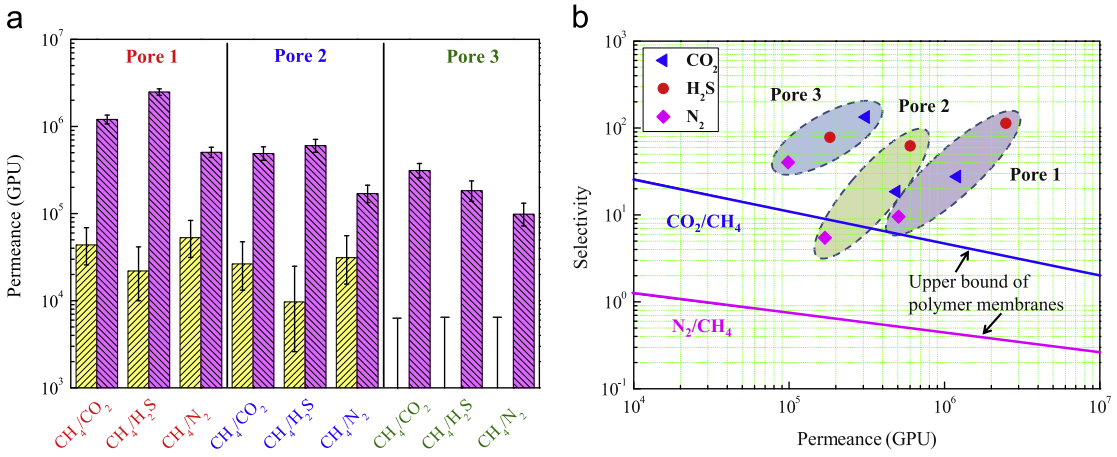

Fig. 4. Separation performance of the gas mixtures involved in this study by the NPG membranes. (a) Permeance of various gases for the NPGs with Pore 1, Pore 2 and Pore 3; (b) relationship between the permeance of permeating gases and the selectivity of permeating gases over the non-permeating gases. To obtain the upper bound of polymer membranes, in the conversion of permeability (in unit of barrer) to permeance (in unit of GPU), we assume the thickness of polymer membranes is 0.1 μm referring to the work by Li et al. (2013).

Acknowledgment

We acknowledge the financial support from National Natural Science Foundation of China for Distinguished Young Scientists (51425603) and key Program no. 51236007. Chengzhen Sun was supported by the Fundamental Research Funds for the Central Universities.

Appendix A. Supplementary material

Supplementary data associated with this article can be found in the online version at doi:10.1016/j.ces.2015.08.049.

References

Azamat, J., Khataee, A., Joob, S.W., 2015. Molecular dynamics simulation of trihalomethanes separation from water by functionalized nanoporous graphene under induced pressure. Chem. Eng. Sci. 127, 285–292.
Bieri, M., Treier, M., Cai, J.M., Ait-Mansour, K., Ruffieux, P., Groning, O., Groning, P., Kastler, M., Rieger, R., Feng, X.L., Mullen, K., Fasel, R., 2009. Porous graphenes: two-dimensional polymer synthesis with atomic precision. Chem. Commun. 45, 6919–6921.
Boutilier, M.S.H., Sun, C., O'Hern, S.C., Au, H., Hadjiconstantinou, N.G., Karnik, R., 2014. Implications of permeation through intrinsic defects in graphene on the design of defect-tolerant membranes for gas separation. ACS Nano 8, 841–849.
Celebi, K., Buchheim, J., Wyss, R.M., Droudian, A., Gasser, P., Shorubalko, I., Kye, J.-I., Lee, C., Park, H.G., 2014. Ultimate permeation across atomically thin porous graphene. Science 344, 289–292.
Dai, J., Yuan, J., Giannozzi, P., 2009. Gas adsorption on graphene doped with B, N, Al, and S: a theoretical study. Appl. Phys. Lett. 95, 232105.
Dasgupta, T., Punnathanam, S.N., Ayappa, K.G., 2015. Effect of functional groups on separating carbon dioxide from CO_2/N_2 gas mixtures using edge functionalized graphene nanoribbons. Chem. Eng. Sci. 121, 279–291.
Drahushuk, L.W., Strano, M.S., 2012. Mechanisms of gas permeation through single layer graphene membranes. Langmuir 28, 16671–16678.
Du, H.L., Li, J.Y., Zhang, J., Su, G., Li, X.Y., Zhao, Y.L., 2011. Separation of hydrogen and nitrogen gases with porous graphene membrane. J. Phys. Chem. C 115, 23261–23266.
Harris, J.G., Yung, K.H., 1995. Carbon dioxides liquid-vapor coexistence curve and critical properties as predicted by a simple molecular-model. J. Phys. Chem. 99, 12021–12024.
Hauser, A.W., Schwerdtfeger, P., 2012. Methane-selective nanoporous graphene membranes for gas purification. Phys. Chem. Chem. Phys. 14, 13292–13298.
Huang, C., Wu, H., Deng, K., Tang, W., Kan, E., 2014. Improved permeability and selectivity in porous graphene for hydrogen purification. Phys. Chem. Chem. Phys. 16, 25755–25759.
Jiang, D.E., Cooper, V.R., Dai, S., 2009. Porous graphene as the ultimate membrane for gas separation. Nano Lett. 9, 4019–4024.
Jiao, Y., Du, A., Hankel, M., Smith, S.C., 2013. Modelling carbon membranes for gas and isotope separation. Phys. Chem. Chem. Phys. 15, 4832–4843.
Kim, H.W., Yoon, H.W., Yoon, S.-M., Yoo, B.M., Ahn, B.K., Cho, Y.H., Shin, H.J., Yang, H., Paik, U., Kwon, S., Choi, J.-Y., Park, H.B., 2013. Selective gas transport through few-layered graphene and graphene oxide membranes. Science 342, 91–95.
Koenig, S.P., Wang, L.D., Pellegrino, J., Bunch, J.S., 2012. Selective molecular sieving through porous graphene. Nat. Nanotechnol. 7, 728–732.
Kwon, H.T., Jeong, H.-K., 2015. Improving propylene/propane separation performance of zeolitic-imidazolate framework ZIF-8 membranes. Chem. Eng. Sci. 124, 20–26.
Lee, J., Aluru, N.R., 2010. Separation of gases from gas-water mixtures using carbon nanotubes. Appl. Phys. Lett. 96, 133108.
Lei, G., Liu, C., Xie, H., Song, F., 2014. Separation of the hydrogen sulfide and methane mixture by the porous graphene membrane: effect of the charges. Chem. Phys. Lett. 599, 127–132.
Li, H., Song, Z., Zhang, X., Huang, Y., Li, S., Mao, Y., Ploehn, H.J., Bao, Y., Yu, M., 2013. Ultrathin, molecular-sieving graphene oxide membranes for selective hydrogen separation. Science 342, 95–98.
Liu, H., Dai, S., Jiang, D., 2013a. Insights into CO_2/N_2 separation through nanoporous graphene from molecular dynamics. Nanoscale 5, 9984–9987.
Liu, H., Dai, S., Jiang, D., 2013b. Permeance of H_2 through porous graphene from molecular dynamics. Solid State Commun. 175–176, 101–105.
Lu, R., Rao, D., Lu, Z., Qian, J., Li, F., Wu, H., Wang, Y., Xiao, C., Deng, K., Kan, E., Deng, W., 2012. Prominently improved hydrogen purification and dispersive metal binding for hydrogen storage by substitutional doping in porous graphene. J. Phys. Chem. C 116, 21291–21296.
Nieszporek, K., Drach, M., 2015. Alkane separation using nanoporous graphene membranes. Phys. Chem. Chem. Phys. 17, 1018–1024.
Robeson, L.M., 2008. The upper bound revisited. J. Membr. Sci. 320, 390–400.
Schrier, J., 2010. Helium separation using porous graphene membranes. J. Phys. Chem. Lett. 1, 2284–2287.
Schrier, J., 2012. Carbon dioxide separation with a two-dimensional polymer membrane. ACS Appl. Mater. Interfaces 4, 3745–3752.
Shan, M., Xue, Q., Jing, N., Ling, C., Zhang, T., Yan, Z., Zheng, J., 2012. Influence of chemical functionalization on the CO_2/N_2 separation performance of porous graphene membranes. Nanoscale 4, 5477–5482.
Sun, C., Boutilier, M.S.H., Au, H., Poesio, P., Bai, B., Karnik, R., Hadjiconstantinou, N. G., 2014. Mechanisms of molecular permeation through nanoporous graphene membranes. Langmuir 30, 675–682.
Sun, C., Wen, B., Bai, B., 2015. Recent advances in nanoporous graphene membrane for gas separation and water purification. Sci. Bull., To appear.
Tao, Y., Xue, Q., Liu, Z., Shan, M., Ling, C., Wu, T., Li, X., 2014. Tunable hydrogen separation in porous graphene membrane: First-principle and molecular dynamic simulation. ACS Appl. Mater. Interfaces 6, 8048–8058.
Walker, M.I., Weatherup, R.S., Bell, N.A.W., Hofmann, S., Keyser, U.F., 2015. Free-standing graphene membranes on glass nanopores for ionic current measurements. Appl. Phys. Lett. 106, 023119.
Wang, E.N., Karnik, R., 2012. Water desalination: graphene cleans up water. Nat. Nanotechnol. 7, 552–554.
Wen, B., Sun, C., Bai, B., 2015. Inhibition effect of a non-permeating component on gas permeability of nanoporous graphene membrane. Phys. Chem. Chem. Phys. 17, 23619–23626.
Wu, T., Xue, Q., Ling, C., Shan, M., Liu, Z., Tao, Y., Li, X., 2014. Fluorine-modified porous graphene as membrane for CO_2/N_2 separation: molecular dynamic and first-principles simulations. J. Phys. Chem. C 118, 7369–7376.
Xu, Q., Xu, H., Chen, J., Dong, C., Sreeprasad, T.S., 2015. Graphene and graphene oxide: advanced membranes for gas separation and water purification. Inorg. Chem. Front. 2, 417–424.
Zhao, Y., Xie, Y., Liu, Z., Wang, X., Chai, Y., Yan, F., 2014. Two-dimensional material membranes: an emerging platform for controllable mass transport applications. Small 10, 4521–4542.